PHYSICAL REVIEW B VOLUME 48, NUMBER 21 1 DECEMBER 1993-I

Oscillatory interlayer coupling and giant magnetoresistance in epitaxial Fe/Cr(211) and (100) superlattices

Eric E. Fullerton, M. J. Conover, J. E. Mattson, C. H. Sowers, and S. D. Bader
Materials Science Division, Argonne National Laboratory, Argonne, Illinois 60439
(Received 14 June 1993)

An epitaxial orientation of Fe/Cr superlattices—Fe/Cr(211) on MgO(110)—is grown by magnetron sputtering. Its structural and magnetic characterizations are presented and compared to those for Fe/Cr(100) superlattices grown simultaneously onto MgO(100) substrates. The epitaxial orientation of the Fe/Cr(211) superlattices is Fe/Cr[0$\bar{1}$1]||MgO[001] and Fe/Cr[$\bar{1}$11]||MgO[1$\bar{1}$0], while that for Fe/Cr(100) is Fe/Cr[001]|| MgO[011]. A uniaxial, in-plane surface anisotropy for the Fe/Cr(211) superlattices along the Fe[0$\bar{1}$1] of 0.06 erg/cm^2 is obtained from analysis of the magnetization hysteresis loops. Four oscillations in the antiferromagnetic interlayer coupling and giant magnetoresistance (GMR) are observed with a period of 18 Å for both orientations. The strength, oscillation period, and phase of the magnetic coupling are identical for the two orientations. The GMR values increase by a factor of ~4 to 5 on cooling from room temperature to 4.2 K. At 4.2 K the maximum GMR value of the [Fe(14 Å)/Cr(8 Å)]$_{50}$ superlattice is 70% for the (211) orientation and 150% for the (100) orientation.

I. INTRODUCTION

Since the discovery of antiferromagnetic (AF) coupling[1] and the corresponding giant magnetoresistance (GMR) effect[2] in Fe/Cr superlattices, there has been considerable experimental[3–14] and theoretical investigation[15–21] of these phenomena. Oscillations in the AF coupling strength and GMR with a period of 18 Å have been observed in sputtered Fe/Cr(110)-textured multilayers.[3] A similar long-period oscillation in the AF coupling was reported for Fe/Cr/Fe(100)-wedged samples prepared at room temperature.[4] When the wedged samples were prepared at elevated temperature, a short period (two monolayers) was observed.[4,5] The two-monolayer oscillations are thought to be directly related to the nested Fermi surface of Cr. The origin of the 18-Å long-period oscillation has been related to a spanning vector of the Cr(100) Fermi surface,[18] but remains an open question. In most transition metals, the long-period oscillation is closer to 11 Å.[14] In order to get deeper insight into the physics of the coupling in this and related systems, a variety of epitaxial orientations should be studied. In this paper we study an epitaxial orientation of Fe/Cr-superlattices: Fe/Cr(211) grown by magnetron sputtering onto MgO(110). We present structural and magnetic properties and compare the results to Fe/Cr(100) superlattices grown simultaneously onto MgO(100) substrates. We emphasize that these samples grow *epitaxially* as single crystals and not just as the textured polycrystals that are more typical of the sputtering process. The epitaxy leads to the stabilization of the unusual (211) low-Miller-index face and to identification of an in-plane surface anisotropy that stabilizes a low-field plateau in the magnetic hysteresis loops. Such features are more commonly encountered in molecular-beam epitaxy (MBE). We also identify four oscillations in the AF coupling and magnetoresistance with a period of 18 Å for both the (211) and (100) superlattices. We find that the strength, oscillation period and phase of the AF coupling are independent of the crystallographic orientation. The GMR does, however, depend on crystallographic orientation; values for the Fe/Cr(100) samples are roughly twice as large as those for the (211) samples. A value of 150% is obtained for the [Fe(14 Å)/Cr(8 Å)]$_{50}$ (100) superlattice at 4.2 K. This is larger than for the MBE samples of Refs. 2 and 10.

To outline the plan of the paper, we present the experimental procedure, structural characterizations, magnetization, and magnetoresistance in Secs. II–V, respectively, discuss the coupling energetics and magnetoresistance in Sec. VI, and summarize major conclusions in Sec. VII.

II. EXPERIMENTAL PROCEDURE

The Fe/Cr superlattices were grown by dc magnetron sputtering onto epitaxially polished single-crystal MgO(110) and MgO(100) substrates. The sputtering chamber had a base pressure of $<5\times10^{-8}$ Torr, and substrates were introduced into the chamber via a load lock. The 2-in. planar magnetron sputtering guns were operated in an Ar pressure of 3 mTorr and a target-substrate distance of 9 cm. The (110) and (100) substrates were mounted side by side onto the sample holder and codeposited. A 100-Å Cr buffer layer was initially deposited at a substrate temperature of 600 °C to establish the epitaxial orientation with the substrate.[22] The substrate was then cooled to 180 °C, and the superlattice was grown by sequential deposition of the Fe and Cr layers. The total number of layers was adjusted so that the total superlattice thickness was constant at ≈1200 Å. The structures were characterized by x-ray diffraction using Cu $K\alpha$ radiation. Magnetic properties were measured by superconducting quantum interference device (SQUID) magnetometry and longitudinal Kerr rotation. Magnetotransport properties were studied by standard four-probe tech-

 ©1993 The American Physical Society

nique using lock-in detection on rectangular pieces of substrate which were cleaved along the [001] and [1$\bar{1}$0] directions for the MgO(110) samples and along the [001] for the MgO(100) samples.

III. X-RAY-DIFFRACTION RESULTS

Shown in Figs. 1 and 2 are representative x-ray-diffraction results for Fe/Cr superlattices on MgO(110) and (100) substrates, respectively. Figure 1(a) shows the low-angle spectrum of an [Fe(14 Å)/Cr(46 Å)]$_{20}$ sample which has six superlattice reflections due to the chemical modulation. The combination of sharp diffraction features with reflections up to sixth order indicates that the layers are smooth and have well-formed interfaces. Rocking curves about the superlattice peaks consist of two components, a sharp specular and broad diffuse component resulting from the interfacial roughness. Longitudinal scans with the scattering vector misaligned from the specular condition (by 0.17°) were strongly peaked at the same angle as the specular scan, indicating that the interfacial roughness is correlated from layer to layer.[23] Rotating the sample 90° did not qualitatively change the diffuse scattering; this implies that there are no qualitative changes in the interfacial morphology along orthogonal directions of the superlattice.

Figure 2(a) shows the low-angle spectrum for the corresponding [Fe(14 Å)/Cr(46 Å)]$_{20}$ sample on MgO(100). The low-angle diffraction peaks decay in intensity faster than in the case of the MgO(110) sample. This indicates that the interfacial roughness and/or interdiffusion is somewhat larger. Rocking curves about the superlattice peaks show a two-component line shape similar to that for the MgO(110) sample. However, the intensity of the diffuse component relative to the specular peak is slightly increased, which indicates a corresponding increase in the interfacial roughness relative to that for the MgO(110) sample.

The high-angle spectra of the same [Fe(14 Å)/Cr(46 Å)]$_{20}$ superlattices are shown in Figs. 1(b) and 2(b). Figure 1(b) contains the MgO(220) substrate reflection and the Fe/Cr(211) reflection flanked by two superlattice peaks. The full width at half maximum (FWHM) of the Fe/Cr(211) reflection $K\alpha_1$ component is 0.27°, which yields a crystal coherence length of ≈400 Å. There is no indication of the presence of Fe/Cr(110) or (200) reflections. Since the Fe/Cr(200) reflection would appear on the tail of the MgO peak, the sample was slightly misaligned to suppress the MgO intensity. But, again, no Fe/Cr(200) reflection was observed. Rocking curves about the Fe/Cr(211) reflection have FWHM that range from 0.6° to 1.1° for various Cr thicknesses, which is indicative of a high degree of crystal orientation. Shown as the inset of Fig. 1(b) is a rocking curve of the Fe/Cr(211) peak, with a FWHM of 0.75°, taken with the in-plane component of the scattering vector parallel to the MgO[001] direction. The rocking curve with the in-plane component parallel to the MgO[1$\bar{1}$0] direction has a FWHM of 1.0°. Fittings of the high-angle diffraction spectra to a general structural model[25,26] yield Fe and Cr(211) lattice spacings of 1.170±0.003 and 1.177±0.002 Å, respectively. Both values agree with the bulk values for Fe and Cr.

Figure 2(b) consists of the MgO(200) and Fe/Cr(200) reflections. No Fe/Cr(110) or (211) reflections were observed. Again, the sample was slightly misaligned to confirm the absence of an Fe/Cr(110) reflection. The Fe/Cr(200) reflection has a FWHM of 0.22°, which corresponds to a crystal coherence of ≈430 Å. The inset shows that the rocking curve about the Fe/Cr(200)

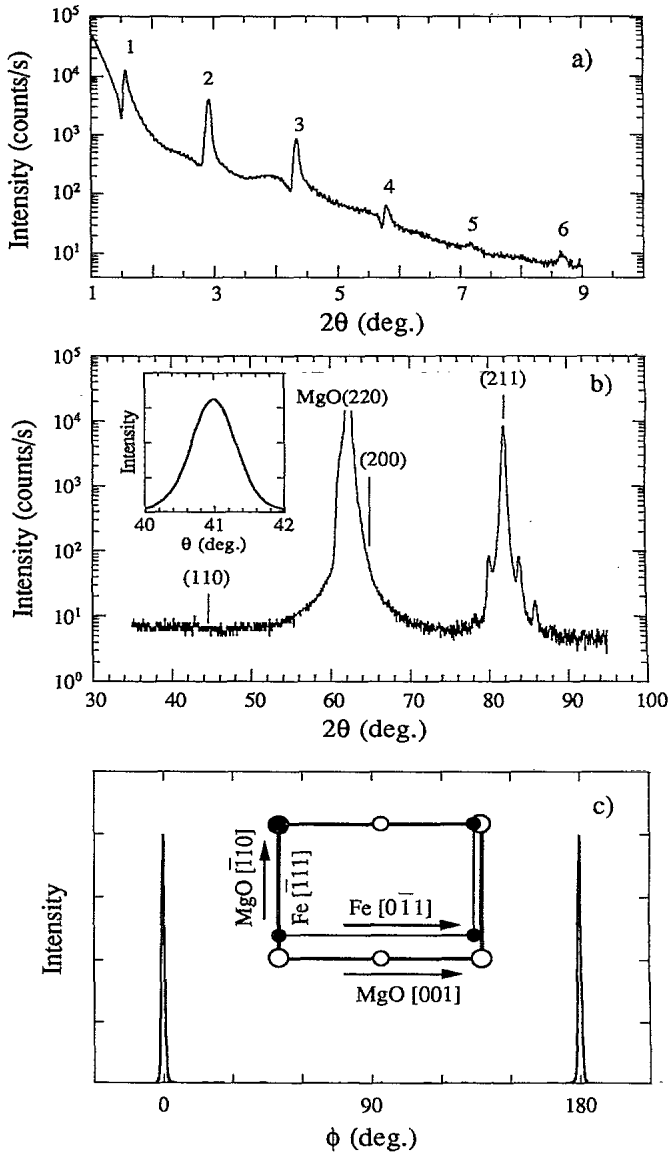

FIG. 1. X-ray-diffraction results for Fe/Cr superlattice grown on MgO(110). (a) Low-angle spectrum for an [Fe(1 Å)/Cr(46 Å)]$_{20}$ superlattice, with Bragg reflections indexed a shown. (b) High-angle spectrum for the same superlattice as i (a). The possible Fe/Cr reflections and the MgO(220) reflection are identified. The inset shows the rocking curve about th Fe/Cr(211) reflection. (c) Fe/Cr(110) intensity as a function c rotation angle ϕ about the surface normal for an [Fe(1 Å)/Cr(17 Å)]$_{36}$ superlattice. The inset shows the epitaxial rela tion of the Fe/Cr superlattice (solid circles) with respect to th MgO substrate (open circles).

reflection has a FWHM of 0.7°. Fittings of the high-angle diffraction spectra yield Fe and Cr lattice spacings of 1.431±0.003 and 1.443±0.003 Å, respectively, in agreement with bulk values. For both substrates, the rocking curves indicate that the superlattices are aligned with the MgO substrate to within $<0.1°$.

The in-plane structure and expitaxial orientation were explored by asymmetric diffraction scans. Figure 1(c) is a ϕ scan of an [Fe(14 Å)/Cr(17 Å)]$_{36}$ superlattice, which shows the measured Fe/Cr(110) intensity while rotating the sample about the surface normal. $\phi=0°$ corresponds to the in-plane component of the scattering vector parallel to the MgO[001] direction. Diffraction peaks at 0° and 180° confirm the expected twofold symmetry of the (211) face epitaxially oriented with the substrate. The FWHM of the ϕ-scan diffraction peak is 1.4°, indicative of a high degree of epitaxy. From the angular position of the peaks, the epitaxial orientations [shown schematically as an inset of Fig. 1(c)] Fe/Cr[0$\bar{1}$1]||MgO[001] and Fe/Cr[$\bar{1}$11]||MgO[1$\bar{1}$0] correspond to a 3.8% and 16.7% lattice mismatch of the Cr with MgO, respectively. The 100-Å Cr base layer should be sufficiently thick to relieve most of the epitaxial strain prior to the growth of the superlattice. The same orientational relationship between Fe and MgO(110) was reported recently for MBE-grown Fe films.[24]

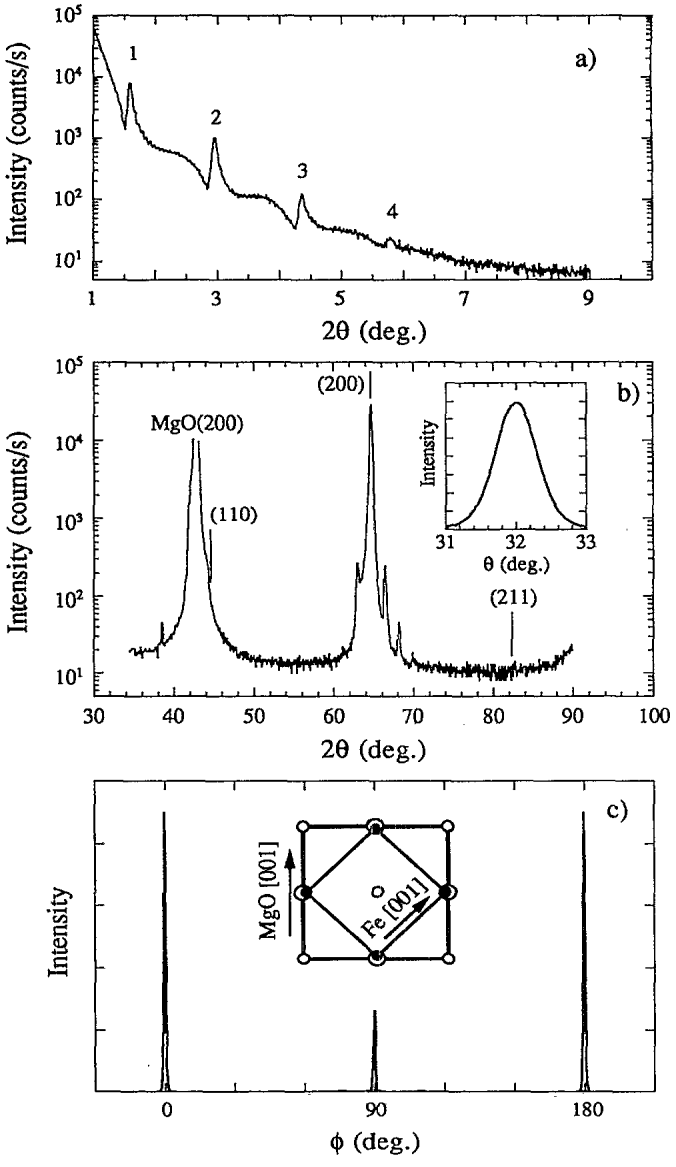

FIG. 2. X-ray-diffraction results for Fe/Cr superlattices grown on MgO(100). (a) Low-angle spectrum for an [Fe(14 Å)/Cr(46 Å)]$_{20}$ superlattice, with Bragg reflections indexed as shown. (b) High-angle spectrum for the same superlattice as in (a). The possible Fe/Cr reflections and the MgO(200) reflections are identified. The inset shows the rocking curve about the Fe/Cr(200) reflection. (c) Fe/Cr(110) intensity as a function of rotation angle ϕ about the surface normal for an [Fe(14 Å)/Cr(17 Å)]$_{36}$ superlattice. The inset shows the epitaxial relation of the Fe/Cr superlattice (solid circles) with respect to the MgO substrate (open circles).

Shown in Fig. 2(c) is the ϕ scan of the Fe/Cr(110) reflection for an [Fe(14 Å)/Cr(17 Å)]$_{36}$ superlattice on MgO(100). The expected fourfold symmetry is observed for the MgO(100) surface, and the FWHM is 1.0°. The peak at 90° is suppressed for clarity. The epitaxial orientation [shown schematically as an inset in Fig. 2(c)] Fe/Cr[010]||MgO[011] corresponds to a 3.8% lattice mismatch of the Cr with the MgO. From the x-ray-diffraction results presented above, *our Fe/Cr-sputtered superlattices on MgO appear comparable in structural quality (epitaxial orientation, mosaic spread, flatness of layers) to those produced by MBE.*

IV. MAGNETIZATION RESULTS

A. Fe/Cr(211)

Shown in Figs. 3(a) and 3(b) are the room-temperature (RT) magnetization hysteresis loops of (211)-oriented [Fe(14 Å)/Cr(38 Å)]$_{22}$ and [Fe(90 Å)/Cr(38 Å)]$_8$, respectively, with the applied field H parallel to the Fe[$\bar{1}$11] and Fe[0$\bar{1}$1] directions. For the 14-Å Fe layer, there is a strong in-plane anisotropy along the Fe[0$\bar{1}$1] direction. To quantify the anisotropy, we analyze the hysteresis loop with H along the hard axis (Fe[$\bar{1}$11]) utilizing an expression which includes a magnetocrystalline anisotropy (K_1) and a uniaxial anisotropy (K_U) along the Fe[0$\bar{1}$1], as well as a Zeeman term ($MH\cos\theta$). The anisotropy energy in the (211) plane is given by[24,27]

$$E=K_1(\cos^4\theta/3+\sin^4\theta/4)+K_U\cos^2\theta\ , \qquad (1)$$

where θ is the in-plane angle between the magnetization and the [$\bar{1}$11] direction. In the absence of K_U, the magnetic easy axis would be $\theta\approx 50°$. Minimizing the total energy [Eq. (1) with the inclusion of a Zeeman term] gives the expression[24]

$$H=\frac{7K_1}{3M_S}\left[\frac{M}{M_S}\right]^3+\frac{2K_U-K_1}{M_S}\frac{M}{M_S}\ , \qquad (2)$$

where M_S is the saturation magnetization. By least-squares fitting the hysteresis loops [Figs. 3(a) and 3(b)] to Eq. (2), the values for K_1 and K_U are determined. The solid lines through the measured hard-axis loops show

the best-fit results for K_1 and K_U. The values for K_1 of 4.2×10^5 and 5.3×10^5 ergs/cm^3 for the 14- and 90-Å Fe layers, respectively, are close to the bulk value of 4.7×10^5 ergs/cm^3. In contrast, the uniaxial term is strongly thickness dependent, as shown in Fig. 3(c). K_U varies inversely with Fe thickness (down to 14 Å), characteristic of a surface anisotropy. Fitting the uniaxial component to the expression $K_U=2K_S/t_{Fe}$ is shown by the solid line in Fig. 3(c) and gives an in-plane surface anisotropy energy of $K_S=0.06$ ergs/cm^2. We should point out that a uniaxial in-plane anisotropy was observed for thick Fe(211) films grown on Cu(110).[27]

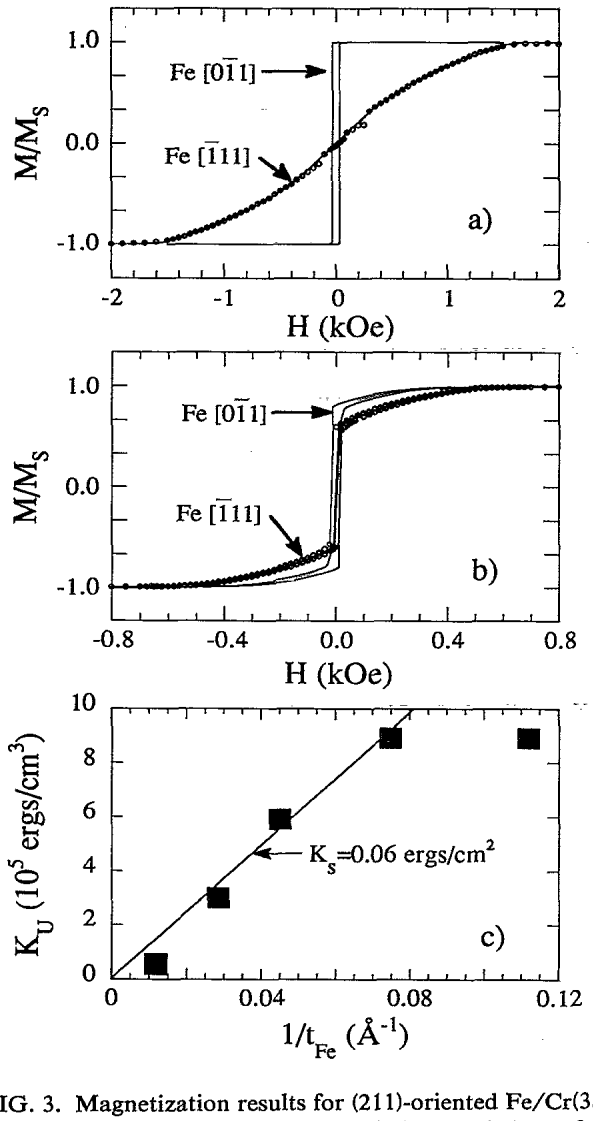

FIG. 3. Magnetization results for (211)-oriented Fe/Cr(38 Å) superlattices on MgO(110). (a) Magnetic hysteresis loops for an [Fe(14 Å)/Cr(38 Å)]$_{22}$ superlattice with H parallel to the Fe[0$\bar{1}$1] and Fe[$\bar{1}$11] directions. (b) Magnetic hysteresis loops for an [Fe(90 Å)/Cr(38 Å)]$_8$ superlattice with H parallel to the Fe[0$\bar{1}$1] and Fe[$\bar{1}$11] directions. For the Fe[$\bar{1}$11] directions, the open circles are the measured points and the solid line represents the best fit to Eq. (2). (c) Uniaxial anisotropy constant K_U determined from the magnetic hysteresis loops vs inverse Fe thickness. The solid line is the expected behavior assuming an in-plane surface anisotropy of 0.06 erg/cm^2.

Shown in Fig. 4 is the RT magnetization hysteresis loops for a representative set of the (211)-oriented Fe(14 Å)/Cr superlattices with various Cr thicknesses. M_S of the Fe layers at RT is independent of Cr thickness and averages to $\approx$1400 emu/cm^3. The loops were measured with H along the easy axis. They show the oscillations in the sign of the magnetic coupling; those to the left in Fig. 4 are characteristic of AF coupling, and those to the right are ferromagnetic or uncoupled. The loop shapes in the left panels are representative of superlattices in which there is a competition between AF coupling of the magnetic layers and a uniaxial in-plane anisotropy. A recent paper by Folkerts[28] presents calculations of the magnetic hysteresis loops for superlattices with various types of anisotropy and AF coupling strengths (J_{AF}). For the case of uniaxial in-plane anisotropy, if $J_{AF}>K_U t_{Fe}$ (e.g., $t_{Cr}=11$ Å in Fig. 4), a plateau will form at low field in which the magnetic layers are AF aligned along the directions of the easy axes. At a higher field, the system undergoes a spin-flop transition and rotates to saturation at the switching field defined by $H_S=4J_{AF}/M_S t_{Fe}-2K_U/M_S$. If $J_{AF}<K_U t_{Fe}$ (e.g., $t_{Cr}=26$ and 46 Å in Fig. 4), then the layers switch from AF alignment to parallel alignment at a field $H_S=2J_{AF}/M_S t_{Fe}$. Similar loop shapes have been observed in CoFe/Cu(110) superlattices grown on MgO(110) substrates.[29] Some caution needs to be used when comparing measured loops with the above expressions since the system in not purely uniaxial; there is the additional magnetocrystalline volume anisotropy contribution. However, for the samples shown in Fig. 4, the uniaxial term dominates. Shown in Fig. 5 is a summary of H_S values determined from the magnetic hysteresis loops. H_S was defined as one-half the field required to switch the magnetization from +90% magnetization to −90% magnetization. For the samples with square hysteresis loops, the switching fields were smaller than the step size of the measurement (5–10 Oe) , and so H_S was set at 5 Oe for these samples. Four oscillations in the AF coupling are observed with the expected period of 18 Å.

B. Fe/Cr(100)

Shown in Fig. 6 are the RT magnetization hysteresis loops for a representative set of the (100)-oriented Fe(14 Å)/Cr superlattices with H parallel to the Fe[$\bar{1}$10] hard axis. The magnetic easy axis is along the Fe[001] for all Fe thicknesses. The average M_S value of $\approx$1400 emu/cm^3 of Fe is similar to that of the Fe/Cr(211) samples. The loops in the left panels represent AF coupling, and those in the right panels represent ferromagnetic or uncoupled cases. Figure 7(a) shows the saturation field and Fig. 7(b) shows the squareness ratio M_R/M_S vs Cr thickness, where M_R is the remanent magnetization. The expected M_R/M_S ratio of 0.71, shown by the arrow in Fig. 7(b), assumes rotation of the magnetization to the Fe[001] easy axis from the Fe[$\bar{1}$10] axis at saturation. Four oscillations are observed in H_S. The phase and period are identical to those for the (211) samples.

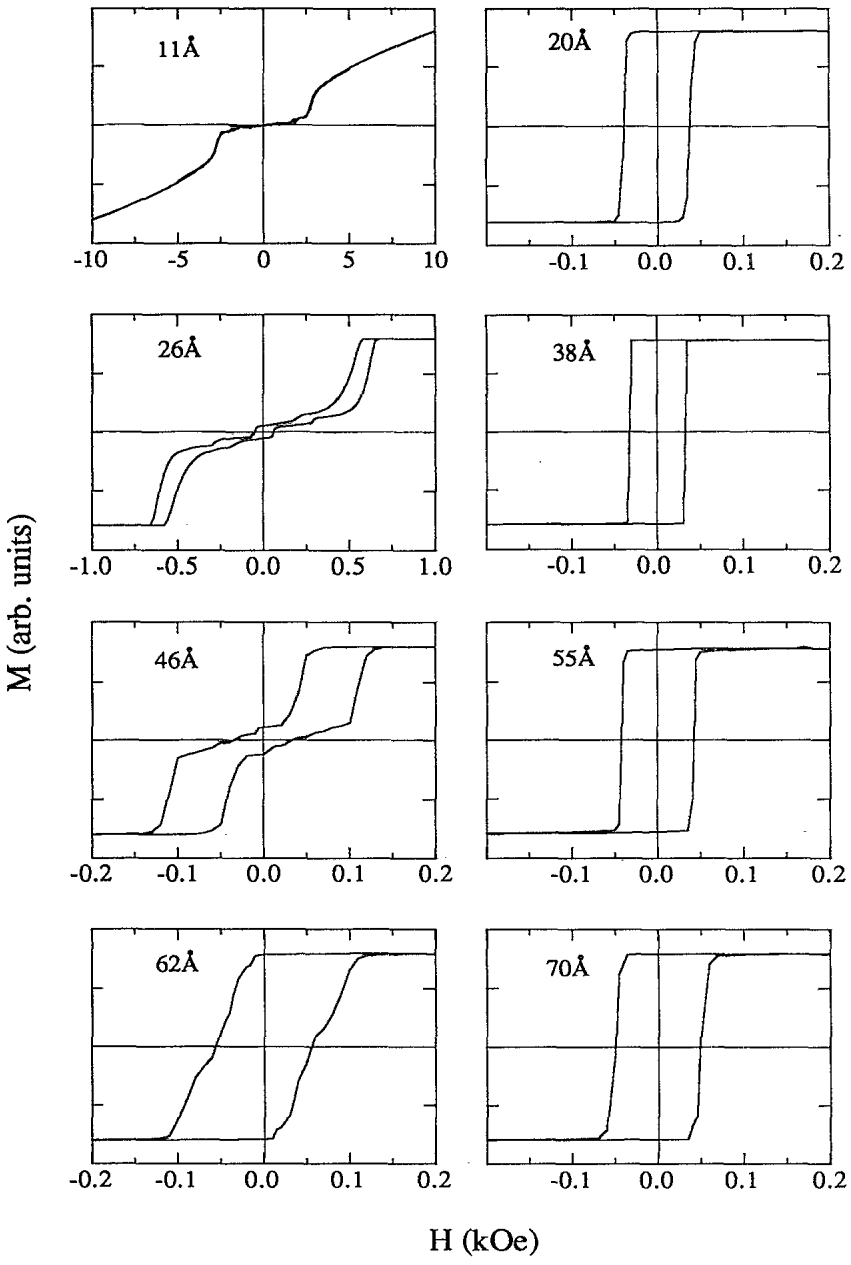

FIG. 4. Magnetic hysteresis loops at RT for (211)-oriented Fe(14 Å)/Cr(t_{Cr}) superlattices with H parallel to the Fe[0$\bar{1}$1] easy axis. The Cr thickness is given in each panel.

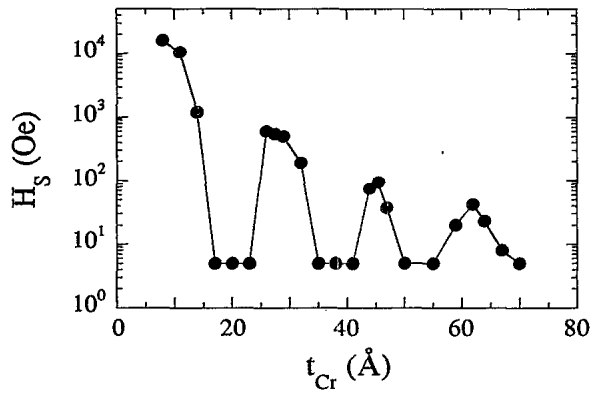

FIG. 5. Switching field H_S for (211)-oriented Fe(14 Å)/Cr(t_{Cr}) superlattices measured at RT with H parallel to the Fe[0$\bar{1}$1] direction.

V. MAGNETORESISTANCE RESULTS

A. Fe/Cr(211)

Figure 8 shows the magnetoresistance (MR) curves for the same AF-coupled samples as in Fig. 4. The MR is defined here as $-\{[R-R(H)]/R\}\times 100\%$, where R is the resistance at saturation. The negative multiplier is to emphasize that the GMR is a negative effect compared to traditional definitions of MR. H and the current are parallel to each other and to the Fe easy and hard directions, respectively, in the two sets of loops presented in each panel of Fig. 8. The shapes of the MR loops are similar to those of the magnetization loops. With H parallel to the easy axis, the plateau at low fields is clearly observed. When the field is aligned along the hard axis, the MR loop is characteristic of continuous rotation of

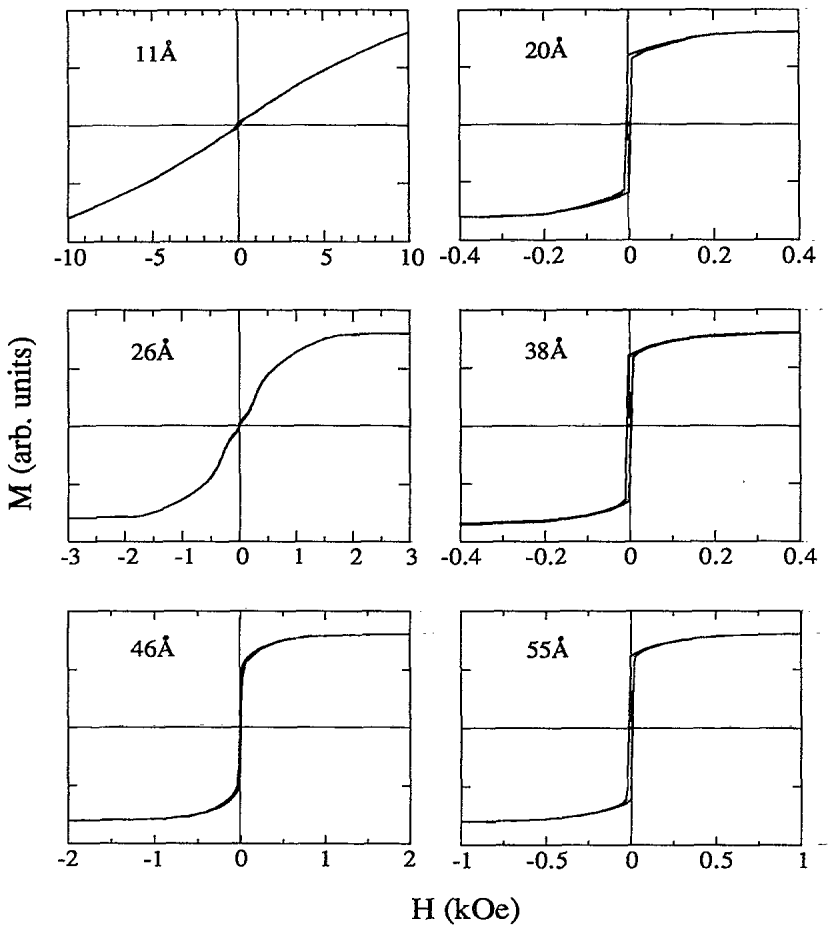

FIG. 6. Magnetic hysteresis loops at RT for (100)-oriented Fe(14 Å)/Cr(t_{Cr}) superlattices with H parallel to the Fe[011] direction. The Cr thickness is given in each panel.

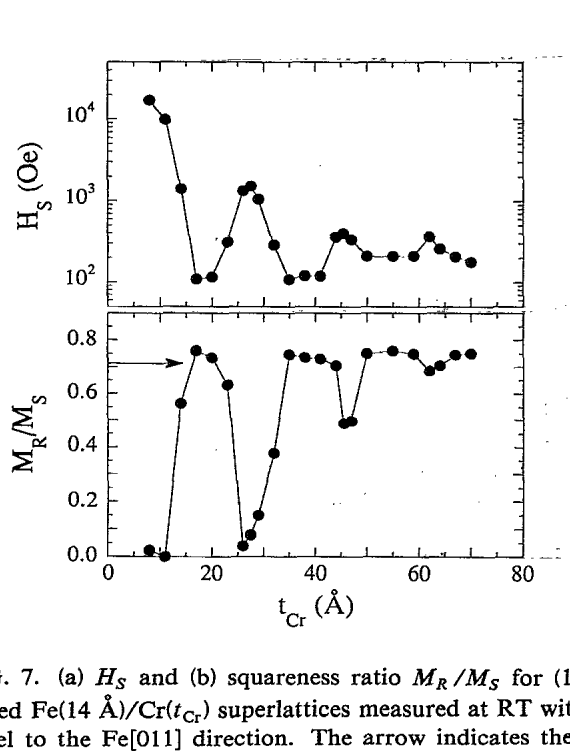

FIG. 7. (a) H_S and (b) squareness ratio M_R/M_S for (100)-oriented Fe(14 Å)/Cr(t_{Cr}) superlattices measured at RT with H parallel to the Fe[011] direction. The arrow indicates the expected squareness ratio assuming no AF coupling.

the layers to saturation. The effect of the uniaxial anisotropy is evident in the different saturation fields for the two orientations. The magnitude of the MR effect also depends on the direction of the current in the sample. When H and the current are oriented along the hard axis, the GMR is consistently $\approx 20\%$ lower in magnitude relative to its value for easy-axis orientation.

The magnetoresistance $\Delta R/R$ is in percentage units, where $\Delta R = R(H=0) - R$. Figure 9 is a plot of $\Delta R/R$ vs Cr thickness which shows four AF oscillations. The saturation resistivity at RT randomly deviates about an average value of 25 $\mu\Omega$ cm for $T_{Cr} > 30$ Å and increases to ≈ 40 $\mu\Omega$ cm for the $t_{Cr} = 8$ Å. The resistivity at 4.2 K is independent of t_{Cr} at a value of ≈ 14 $\mu\Omega$ cm. The resulting residual resistance ratio $\rho(300\text{ K})/\rho(4\text{ K})$ is ≈ 1.7 for the thicker Cr layers and increases to 2.3 for the $t_{Cr} = 8$ Å sample. The magnitude of the GMR (or $\Delta R/R$ at the AF-coupled peaks) decays exponentially with Cr thickness. Fitting the GMR to the expression $A\exp(-t_{Cr}/\lambda^*)$, a value for the effective mean free path λ^* of 14 Å is obtained. The GMR at 4.2 K is also included in Fig. 9 for the relevant AF-coupled samples. The maximum GMR for the [Fe(14 Å)/Cr(8 Å)]$_{50}$ superlattice is 70% at 4.2 K. The GMR increases by a factor of ~ 4–5 on cooling from RT, while λ^* does not change significantly with temperature. However, for low temperatures (< 50 K), the increased coercivity of the Fe layers results in the weakly coupled samples ($t_{Cr} > 40$ Å) no

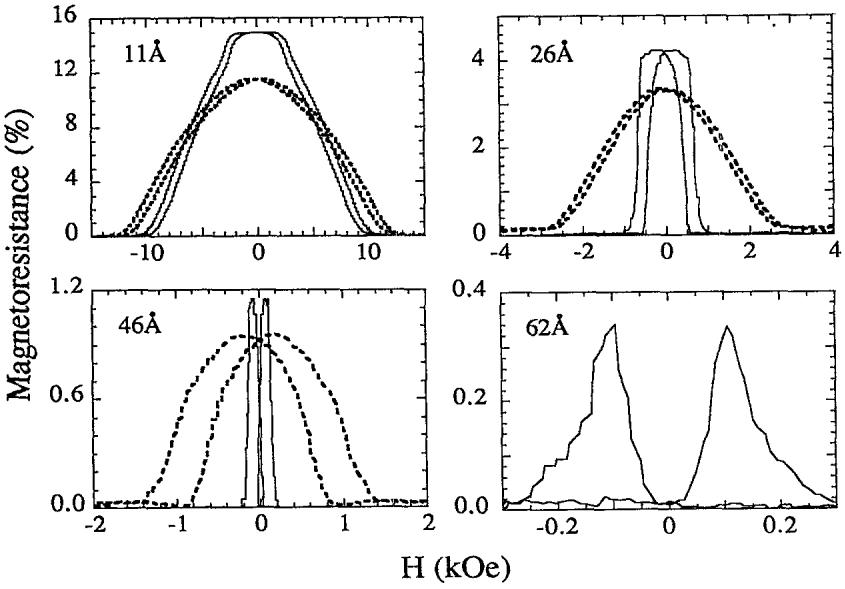

FIG. 8. MR loops at RT with H parallel to the current for the AF-coupled samples of Fig. 4. The dashed line is for the current along the hard axis [$\bar{1}11$] and the solid line along the easy axis [$0\bar{1}1$].

longer becoming completely AF aligned. This phenomenon can be understood from theoretical calculations which show that for coherent rotation of the Fe layers (as opposed to domain wall motion), when $J_{AF}/K_U t_{Fe} < \frac{1}{3}$, the system will switch from $+M_S$ to $-M_S$ at the coercive field and bypass the AF configuration of the Fe layers. The GMR at the third and fourth oscillations, therefore, may be reduced relative to its magnitude for complete AF alignment of the layers.

B. Fe/Cr(100)

The resistivity values for the Fe/Cr(100) samples are very similar to those for the (211) samples. The samples have a slightly increased residual resistance ratio of ≈ 2.0 for the thicker Cr layers and 2.7 for the $t_{Cr} = 8$ Å sample. Shown in Fig. 10(a) are the MR curves for the [Fe(14 Å)/Cr(8)]$_{50}$ superlattice measured at RT and 4.2 K. The most striking feature is the magnitude of the GMR: 150% at 4.2 K and 30% at RT. These values are roughly

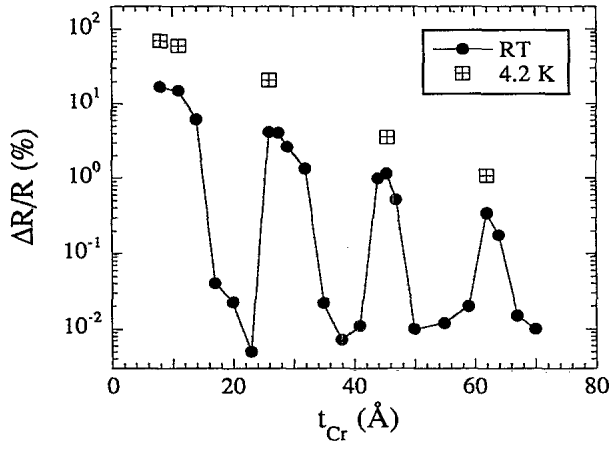

FIG. 9. $\Delta R/R$ vs t_{Cr} for (211)-oriented Fe(14 Å)/Cr(t_{Cr}) superlattices measured at RT and 4.2 K.

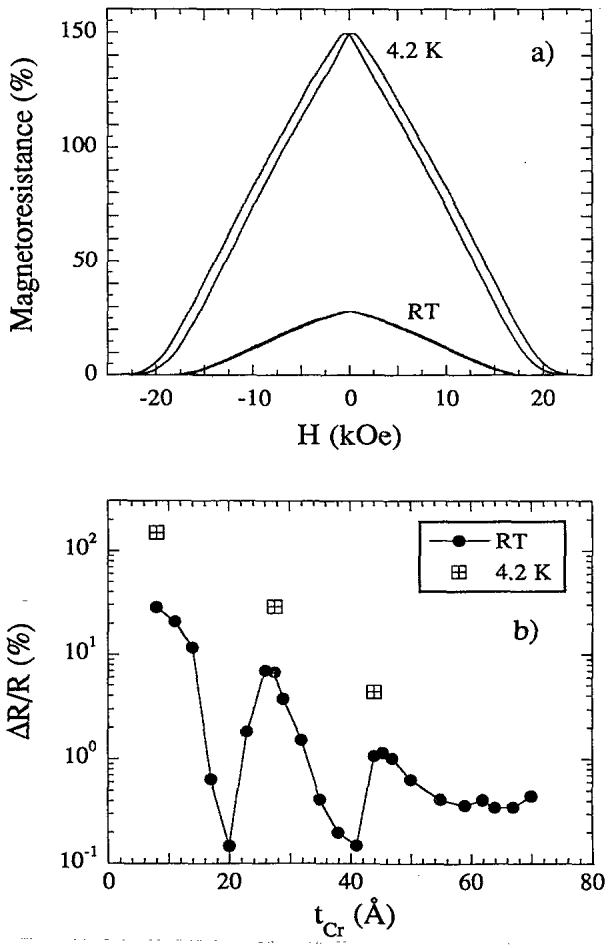

FIG. 10. (a) MR loop for a (100)-oriented [Fe(14 Å)/Cr(8 Å)]$_{50}$ superlattice measured at RT and 4.2 K. (b) $\Delta R/R$ vs t_{Cr} for (100)-oriented Fe(14 Å)/Cr(t_{Cr}) superlattices measured at RT and 4.2 K.

twice as large as those of the corresponding (211) samples; *to our knowledge, the 150% value represents the largest GMR for any superlattice system to date.*[2,10,11,30] Figure 10(b) is a plot of the MR vs Cr thickness showing three oscillations. The fourth oscillation is not convincingly resolved, which most likely results from the high squareness ratio observed in Fig. 7(b) for the fourth oscillation. As was observed in the (211) samples, there is roughly a factor of 4–5 increase in MR with decreasing temperature from RT to 4.2 K. This large increase in MR with decreasing temperature results from both the decrease in ρ and increase in $\Delta\rho$ with decreasing temperature. The changes in $\Delta\rho$ have been related to magnon spin-flip scattering.[7] We should point out that the measured value for the MR is somewhat reduced from its true value as a result of the Cr base layer which shunts some of the current.

VI. DISCUSSION

We first consider the coupling energetics and then discuss the magnetotransport results. A striking observation is that the phase and period of the AF oscillations for the Fe/Cr(211) and Fe/Cr(100) superlattices are identical. The results of the present study are also in accord with the results for the long-period oscillations in Fe/Cr(100)/Fe wedges and for textured Fe/Cr(110) superlattices. This suggests that the long-period oscillation in Cr is independent of the crystallographic orientation of the spacer layer. It is also interesting to explore the orientational dependence of the strength of the AF coupling. This requires converting the saturation fields in Figs. 5 and 7(a) into coupling energies J_{AF} by the expressions[28]

$$J_{AF}(211)=\begin{cases}\dfrac{(H_S+H_K)M_S t_{Fe}}{4} & \text{for } J_{AF}>K_U t_{Fe}\ ,\\ \dfrac{H_S M_S t_{Fe}}{2} & \text{for } J_{AF}<K_U t_{Fe}\ ,\end{cases} \tag{3}$$

$$J_{AF}(100)=\frac{(H_S-H_K)M_S t_{Fe}}{4}\ , \tag{4}$$

where H_K is the anisotropy field given by $2K_U/M_S$ for the (211) samples and $2K_1/M_S$ for the (100) samples. Because H_S is determined with H parallel to the easy and hard directions for the (211) and (100) orientations, respectively, the contribution of H_K in Eqs. (3) and (4) enters with an opposite sign. The calculated values for J_{AF} are shown in Fig. 11, where H_K for both orientations were determined from the saturation field of ferromagnetically coupled samples with neighboring Cr thicknesses. We assume that any thusly derived value of $J_{AF}<10^{-3}$ ergs/cm^2 represents either a ferromagnetic or uncoupled case and show only clearly AF-coupled samples in Fig. 11. As can be seen in Fig. 11, in addition to the phase and period of the oscillations, *the strength of the coupling is independent of the crystallographic orientation.* This result is insensitive to the criterion used for H_S.

There is strong theoretical support for the idea that the

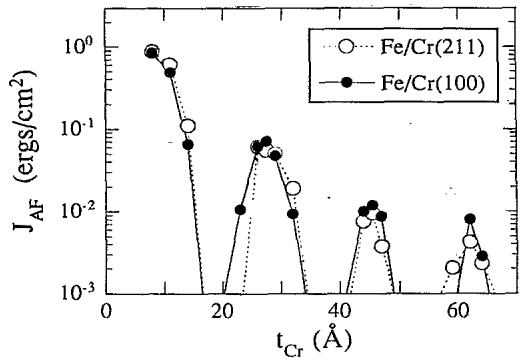

FIG. 11. Antiferromagnetic coupling strength J_{AF} vs t_{Cr} for (211)- and (100)-oriented Fe(14 Å)/Cr(t_{Cr}) superlattices measured at RT.

short-period oscillations observed in a number of systems [e.g., Fe/Cr,[4,5] Co/Cu,[31] Fe/Mn,[32] Fe/Mo (Ref. 33)] depend on the crystal orientation. The dependence is understood to arise within a band-structure-modified Ruderman-Kittel-Kasuya-Yosida (RKKY) framework from spanning vectors which join extremal points of the bulk Fermi surface of the spacer projected along the direction normal to the layers.[15–17] The strength of the coupling is determined theoretically by matrix elements which couple these pairs of points on the Fermi surface. However, experimentally the phase and coupling strength also will be affected by the structure of the interfaces. For a spacer material with a complex Fermi surface, such as a transition metal like Cr, the phase, period, and strength of the coupling are anticipated to depend strongly on the crystallographic orientation. In various theoretical treatments, the long-period oscillation is thought to result from short spanning vectors or equivalently to discrete sampling of shorter oscillations (aliasing) in perfectly ordered layers. The observed period is also thought to depend on roughening of the layers which tends to wash out the short period by averaging over variable layer thicknesses. However, the period and strength of the coupling should still exhibit a dependence on crystallographic orientation. Given this expectation, the results in Fig. 11 are very surprising indeed. However, our empirical observation is similar to that reported for the Co/Cu system, whose long-period oscillation associated with each of the low-Miller-index orientations [(100), (110), and (111)] is nearly constant at $\approx 11-14$ Å.[14,16,34–36]

A second interesting result of the present study concerns the large GMR values observed and, in particular, the 150% value observed for the (100)-oriented sample. A number of groups have reported that the GMR value in Fe/Cr superlattices is enhanced significantly for epitaxially deposited samples.[2,10] This most likely results from the elimination of grain boundaries and other defects that reduce the electron mean free path, as well as from improvements in the structural integrity of the interfaces. This viewpoint applies well to the present results in that both orientations have higher GMR values than most sputtered Fe/Cr superlattices which are polycrystalline and textured. For the first two oscillations,

the GMR values of the Fe/Cr(100) samples are considerably higher than those of the corresponding (211) samples. An interesting issue is whether this difference is intrinsic to the (211) and (100) orientations or results from extrinsic factors such as interfacial morphology[6,8] and/or crystalline quality.[12] Detailed characterizations of the specular and diffuse x-ray scattering, studied at an absorption edge of each of the constituent materials, should be useful to address this in the future.

VII. SUMMARY OF CONCLUSIONS

We report the achievement of epitaxy in the sputtering of Fe/Cr superlattices onto MgO single-crystalline substrates. We introduce an epitaxial orientation of the Fe/Cr system: (211) by growth onto MgO(110). We then make detailed comparisons of the magnetic coupling energetics and magnetoresistance of Fe/Cr(211) with Fe/Cr(100) superlattices grown simultaneously onto MgO(100) substrates. The epitaxial orientation of the Fe/Cr(211) superlattices is Fe/Cr[$0\bar{1}1$]||MgO[001], while that for Fe/Cr(100) is Fe/Cr[001]||MgO[011]. Six low-angle x-ray-diffraction peaks are observed for the (211) superlattice, which is indicative of well-layered films. The magnetic easy axis is along the Fe[$0\bar{1}1$] for the (211) samples, and the [001] for the (100) samples and the hard axes are [$\bar{1}11$] and [$\bar{1}10$], respectively. Fitting the hard-axis magnetization loops yields magnetocrystalline anisotropy energy values that are comparable to that for bulk Fe. Also, an in-plane surface anisotropy of 0.06 erg/cm^2 is extracted for the (211) samples; it imparts a low-field plateau to the hysteresis loops for AF-coupled samples with H aligned with the easy axis. The interlayer magnetic coupling oscillates in sign between ferromagnetic and AF as a function of Cr spacer thickness, and four AF regions are identified via magnetization and MR measurements. The AF coupling period, phase, and strength for both orientations are identical and coincide with the known 18-Å "long-period" oscillation. The GMR values for both orientations increase by a factor of ~4–5 upon cooling from RT to 4.2 K. There is a 20% decrease in the GMR when the field and current are aligned along a hard axis as opposed to an easy axis. The maximum GMR value at 4.2 K for the (211) orientation is 70% and for the (100) orientation is 150% for Fe(14 Å)/Cr(8 Å) samples.

ACKNOWLEDGMENTS

This work was supported by the U.S. Department of Energy, Basic Energy Sciences–Materials Sciences, under Contract No. W-31-109-ENG-38. We would like to thank Mark Beno for assistance in asymmetric diffraction scans.

[1]P. Grünberg, R. Schreiber, Y. Pang, M. B. Brodsky, and C. H. Sowers, Phys. Rev. Lett. **57**, 2442 (1986).
[2]M. N. Baibich, J. M. Broto, A. Fert, F. Nguyen Van Dau, F. Petroff, P. Etienne, B. Greuzet, A. Friederich, and J. Chazelas, Phys. Rev. Lett. **61**, 2472 (1988).
[3]S. S. P. Parkin, N. More, and K. P. Roche, Phys. Rev. Lett. **64**, 2304 (1990).
[4]J. Unguris, R. J. Celotta, and D. T. Pierce, Phys. Rev. Lett. **67**, 140 (1991).
[5]S. T. Purcell, W. Folkerts, M. T. Johnson, N. W. E. McGee, K. Jager, J. ann de Stegge, W. B. Zeper, W. Hoving, and P. Grünberg, Phys. Rev. Lett. **67**, 903 (1991).
[6]E. E. Fullerton, D. M. Kelly, J. Guimpel, I. K. Schuller, and Y. Bruynseraede, Phys. Rev. Lett. **68**, 859 (1992).
[7]J. E. Mattson, M. E. Brubaker, C. H. Sowers, M. Conover, Z. Qiu, and S. D. Bader, Phys. Rev. B **44**, 9378 (1991).
[8]F. Petroff, A. Barthélémy, A. Hamzic, A. Fert, P. Etienne, S. Lequien, and G. Greuzet, J. Magn. Magn. Mater. **93**, 95 (1991).
[9]A. Chaiken, T. M. Tritt, D. J. Gillespie, J. J. Krebbs, P. Lubitz, M. Z. Harford, and G. A. Prinz, J. Appl. Phys. **69**, 4798 (1991).
[10]W. Folkerts, W. Hoving, and W. Coene, J. Appl. Phys. **71**, 362 (1992).
[11]M. A. M. Gijs, S. K. J. Lenczowski, and J. B. Giesbers, Phys. Rev. Lett. **70**, 3343 (1993).
[12]S. S. P. Parkin and B. R. York, Appl. Phys. Lett. **62**, 1842 (1993).
[13]A. Kamijo and H. Igarashi, J. Appl. Phys. **72**, 3497 (1992).
[14]S. S. P. Parkin, Phys. Rev. Lett. **67**, 3598 (1991).
[15]Y. Wang, P. M. Levy, and J. L. Fry, Phys. Rev. Lett. **65**, 2732 (1990).
[16]P. Bruno and C. Chappert, Phys. Rev. Lett. **67**, 1602 (1991); Phys. Rev. B **46**, 261 (1992).
[17]F. Herman and R. Schrieffer, Phys. Rev. B **46**, 5806 (1992).
[18]M. D. Stiles, Phys. Rev. B **48**, 7238 (1993).
[19]R. Q. Hood and L. M. Falicov, Phys. Rev. B **46**, 8287 (1992).
[20]R. E. Camley and J. Barnás, Phys. Rev. Lett. **63**, 664 (1989).
[21]P. M. Levy, S. Zhang, and A. Fert, Phys. Rev. Lett. **65**, 1643 (1990); S. Zhang, P. M. Levy, and A. Fert, Phys. Rev. B **45**, 8689 (1992).
[22]B. M. Lairson, M. R. Visokay, R. Sinclair, and B. M. Clemens, Appl. Phys. Lett. **61**, 1390 (1992).
[23]S. K. Sinha, Physica B **173**, 25 (1991).
[24]A. Marty, B. Gilles, J. Eymery, A. Chamberod, and J. C. Joud, J. Magn. Magn. Mater. **121**, 57 (1993).
[25]E. E. Fullerton, I. K. Schuller, H. Vanderstraeten, and Y. Bruynseraede, Phys. Rev. B **45**, 9292 (1992).
[26]E. E. Fullerton, I. K. Schuller, and Y. Bruynseraede, MRS Bull. **17**(12), 33 (1992).
[27]Y. Ueda and M. Takahashi, J. Magn. Magn. Mater. **71**, 212 (1988).
[28]W. Folkerts, J. Magn. Magn. Mater. **94**, 302 (1991).
[29]K. Inomata and Y. Saito, Appl. Phys. Lett. **61**, 726 (1992).
[30]S. S. P. Parkin, Z. G. Li, and D. J. Smith, Appl. Phys. Lett. **58**, 2710 (1991).
[31]M. T. Johnson, S. T. Purcell, N. W. E. McGee, R. Coehoorn, J. ann de Stegge, and W. Hoving, Phys. Rev. Lett. **68**, 2688 (1992).
[32]S. T. Purcell, M. T. Johnson, N. W. E. McGee, R. Coehoorn, and W. Hoving, Phys. Rev. B **45**, 13 064 (1992).
[33]Z. Q. Qiu, J. Pearson, A. Berger, and S. D. Bader, Phys. Rev. Lett. **68**, 1398 (1992).
[34]M. T. Johnson, R. Coehoorn, J. J. de Vries, N. W. E. McGee, J. ann de Stegge, and P. J. H. Bloemen, Phys. Rev. Lett. **69**, 969 (1992).
[35]F. Herman, M. Van Schilfgaarde, and J. Sticht, Int. J. Mod. Phys. B **7**, 425 (1992).
[36]Z. Q. Qiu, J. Pearson, and S. D. Bader, Phys. Rev. B **46**, 8659 (1992).